Reactive & Functional Polymers 72 (2012) 765–772

Contents lists available at SciVerse ScienceDirect

Reactive & Functional Polymers

journal homepage: www.elsevier.com/locate/react

Early stage evolution of structure and nanoscale property of nanofibers in thermally induced phase separation process

Jundong Shao, Cong Chen, Yingjun Wang, Xiaofeng Chen, Chang Du *

School of Materials Science and Engineering, South China University of Technology, Guangzhou 510641, PR China
National Engineering Research Center for Tissue Restoration and Reconstruction, Guangzhou 510006, PR China

ARTICLE INFO

Article history:
Received 10 December 2011
Received in revised form 9 July 2012
Accepted 23 July 2012
Available online 31 July 2012

Keywords:
Poly(L-lactic acid) nanofibers
Thermally induced phase separation
AFM

ABSTRACT

The structural evolution and nanoscale properties of PLLA nanofiber during the early quenching period in a thermally induced phase separation process have been investigated. The PLLA/THF solution was prepared at 60 °C and quenched in a −24 °C refrigerator for different times to become a gel. The morphology, phase transition, crystallization behavior, hydrophobicity, variation of chain conformation and adhesion force were studied by using SEM, WAXD, ATR-FTIR, DSC, contact angle measurement, AFM and force spectroscopy measurements. The initial phase separation resulted in an amorphous gel with the condensation of nanoparticles, followed by the nucleation of PLLA crystals. The α-form crystal appeared after quenching for 1 min, corresponding to a gel temperature around 15 °C. After quenching for sufficient time (longer than 3 min) and the gel temperature decreasing to below 0 °C, a nanofibrous architecture was formed with a limited disorder α′-form crystal. With the extending of the gelation time, the degree of crystallinity of the matrix increased and conformational transformation of the polymer chains proceeded with more closely packed polymer segments that restricted the backbone C—O—C vibration and strengthened interchain interaction of the C=O bonds. The surface morphology and structural evolution led to the increase in the hydrophobicity as well as nanoscale mechanical property of the nanofibers. AFM and force spectroscopy measurements of 2-D samples on the glass slide showed that the nanofiber formation seemed to initiate from a central nuclei and grew radially outward and larger fibers were assembled laterally with a bunch of thinner nanofibers. The adhesion force increased with the gelation time which suggested that the structural evolution of PLLA chains conformation and the chain packing has a direct functional consequence in the nanoscale mechanical property.

1. Introduction

Nanofibers of various biocompatible materials have been widely studied for applications in tissue engineering [1]. With a high porosity and a large surface area, these nanofibrous scaffolds have been found to promote cell adhesion, proliferation, differentiation and the expression of cell functions [2–5]. Three major techniques are currently employed to produce nanofibers from a wide variety of materials. Self-assembly of peptide-amphiphile [6], block copolymers [7,8] and dendrimers [9] can typically create thinner fibrils with diameters of a few to tens of nanometers. Electrospinning of polycaprolactone (PCL), poly-lactic-co-glycolic acid (PLGA), poly(L-lactic acid) (PLLA) and other synthetic or natural polymers can routinely fabricate larger nanofibers to micron scale fibers [10–12]. Phase separation process has been used to produce nano-fibrous PLLA [13–16] and polyhydroxyalkanoate (PHA) [17] porous scaffolds that mimic the size and scale of extracellular matrix (ECM) component such as the fibrillar structure of collagen (50–500 nm in diameter) [18]. This latter approach is based on the thermodynamic demixing of a homogeneous polymer–solvent system into a polymer-rich phase and a polymer-poor phase, usually by either cooling the solution below a binodal solubility curve or exposure of the solution to an additional immiscible solvent. The thermally induced phase separation (TIPS) process is proposed to occur through spinodal liquid–liquid phase separation and a consequential crystallization of the polymer-rich phase [14,15], but the detailed mechanism is still not fully understood.

Poly(L-lactic acid) (PLLA), as a biodegradable and biocompatible polymer has been attracting much attention from the academic viewpoint of structural interest as well as for practical applications. As a semicrystalline polymer, the crystallization behavior and crystal structure of PLLA have been widely studied. PLLA can form three kinds of crystal modifications (α-, β-, and γ-form) [19–22] depending on the preparation conditions. As the most common and stable one, α-form, with a 10_3 helical chain conformation [22], is generally crystallized from the melt [19,20] or solution [21]. The β-form is obtained under a high drawing radio and high temperature

* Corresponding author. Tel.: +86 020 22236062; fax: +86 020 22236088.
E-mail address: duchang@scut.edu.cn (C. Du).

1381-5148/$ - see front matter © 2012 Elsevier Ltd. All rights reserved.
http://dx.doi.org/10.1016/j.reactfunctpolym.2012.07.011

[20,22], whereas γ-form can be produced via epitaxial crystallization on the hexamethylbenzene substrate [23]. Furthermore, a new crystal α′-form has been reported as a limited disorder crystalline modification of α-form. In melt crystallization, the α′-form appeared at lower crystallization temperature (T_c < 100 °C) compared to the α-form (T_c > 120 °C) [24–31]. The chain conformation and chain-packing mode of α-form and α′-form are slightly different which has been confirmed by the previous analysis. Pan et al. proposed that the α′-form crystal exists widely in the PLLA-based products because of its low crystallization temperature [26–28]. However, few studies have been reported on the crystallization of PLLA from solution via the TIPS process and the formation mechanism of the α′-form crystals from solution still remain unclear.

The morphology, crystallization process, crystal structure, thermal properties and conformational structure of the nanofibrous scaffolds are usually investigated by scanning electron microscopy, X-ray diffraction, differential scanning calorimetry and Fourier-transform infrared spectroscopy [15,32]. The atomic force microscope (AFM) has been used to investigate the elastic modulus of a single nanofiber by a nanoscale three-point bend test [33]. Nanoindentation study provided similar important information about the mechanical properties of nanofibers, such as the elastic modulus and the hardness [34,35]. Force curve analysis and force-mapping have been widely applied to obtain the distribution of sample surface mechanical properties and the surface hydrophilicity at the microscopic level by mapping the adhesion force [36,37].

It is known that properties of PLLA, for instance, its biodegradability, greatly depend on the morphological and structural characteristics. Understanding the phase behavior and crystallization during PLLA nanofiber formation is of fundamental importance. In this study, we focused on the early stage of thermally induced phase separation and gelation process by investigating the structural evolution and nanoscale mechanical property of PLLA nanofibers.

2. Experimental section

2.1. Materials

Poly(L-lactic acid) with an inherent viscosity of 2.4 dl/g was purchased from DaiGang Biomaterial Co. Ltd. (Shandong, China). Tetrahydrofuran (THF) was from DAMAO REAGENT (Tianjin, China). Deionized water was obtained with a Milli-Q water filter system from Millipore Corporation (France). All reagents were used directly without any further purification.

2.2. Preparation procedures

The preparation of PLLA nanofibers through TIPS process follows the procedures of Ma and Zhang [15]. In brief, a 4% (w/v) homogeneous polymer solution was prepared by dissolving PLLA in THF and stirring with a magnetic stirrer at about 60 °C for 2 h. The aliquots of the solution were rapidly transferred into a freezer at a temperature of −24 °C and kept for 1 min, 3 min, 5 min, 10 min, 20 min and up to 2 h, respectively. The temperature decreasing profile of the sample was recorded by using one of the aliquots of the PLLA/THF solution. After quenching for 1 min, the temperature of the solution dropped to about 15 °C, and the temperature further decreased to about 0 °C after 2.5 min, then reached to about −20 °C after 5 min. Solvent exchange was performed at 4 °C after quenching and the water was changed three times a day for 2 days. The resultant sample was freeze-dried for 48 h. The gelation point of 4% (w/v) PLLA/THF solution was about 25 °C [16] and the gelation occurred within several minutes at −24 °C [15].

A diluted 0.5% (w/v) PLLA/THF solution was prepared to cast 2-D samples on the glass slide for the AFM characterization. A series of samples with different quenching time (30 s, 1 min, 2 min, 5 min, 10 min and 20 min) at −24 °C were obtained following the same procedures.

2.3. Scanning electron microscopy (SEM)

The morphology of 3-D scaffolds was observed by Scanning Electron Microscope (Quanta 200, FEI, The Netherlands) at 15 kV by coating with gold in a sputtering device for 1.5 min.

2.4. Wide-angle X-ray diffraction (WAXD)

WAXD patterns were measured by a D8 ADVANCE (Bruker, Germany), with Cu Kα radiation (λ = 0.1542 nm), worked at 40 kV and 40 mA in the scattering angle range of 2θ = 5–50° under the ambient conditions.

2.5. Differential scanning calorimetry (DSC)

Thermal analysis of PLLA scaffolds (sample weight: ca. 6 mg) were carried out with a DIAMOND DSC apparatus, under a nitrogen purge in the temperature range from room temperature to 200 °C at a heating rate of 10 °C/min.

2.6. Attenuated total reflectance FTIR (ATR-FTIR)

ATR-FTIR analysis was performed by a Nicolet, CCR-1 spectrometer at room temperature. A zinc selenide (ZnSe) internal reflection element with a fixed angle of incidence of 45° was used for ATR-FTIR measurements. ATR-FTIR spectra were derived from 64 scans, collected at a resolution of 2 cm^{-1}.

2.7. Contact angle measurement

Contact angle of water droplet was measured by sessile drop method using contact angle goniometer OCA20LHT-TEC700-HTFC1500 (Dataphysics, Germany).

2.8. Atomic force microscopy (AFM)

AFM imaging was conducted using a MFP-3D (Asylum Research, USA) under AC mode in air. Force spectroscopy measurements were performed under contact mode using silicon nitride probes with a spring constant of 1.39 nN/nm.

3. Results and discussion

3.1. SEM study of 3-D scaffolds

Fig. 1 shows scanning electron microscopy (SEM) images of the various samples. After quenching for 1 min, the sample exhibited a relatively dense morphology with some platelet-like structure embedded in an amorphous matrix (Fig. 1a). An irregular nanofibrous network started to form after 3 min gelation. With the increase of the gelation time, the nanofibers tended to be more uniform but there were no significant variations in morphology (Fig. 1b–f). The fiber diameter varied from 50 nm to 500 nm after 2 h gelation. The observation suggested a temperature dependent phase behavior during the early quenching period. We further conducted detail investigations on these samples in terms of the phase transition, crystallization behavior, and changes in crystal structure using WAXD, ATR-FTIR, DSC and Contact angle measurement respectively.

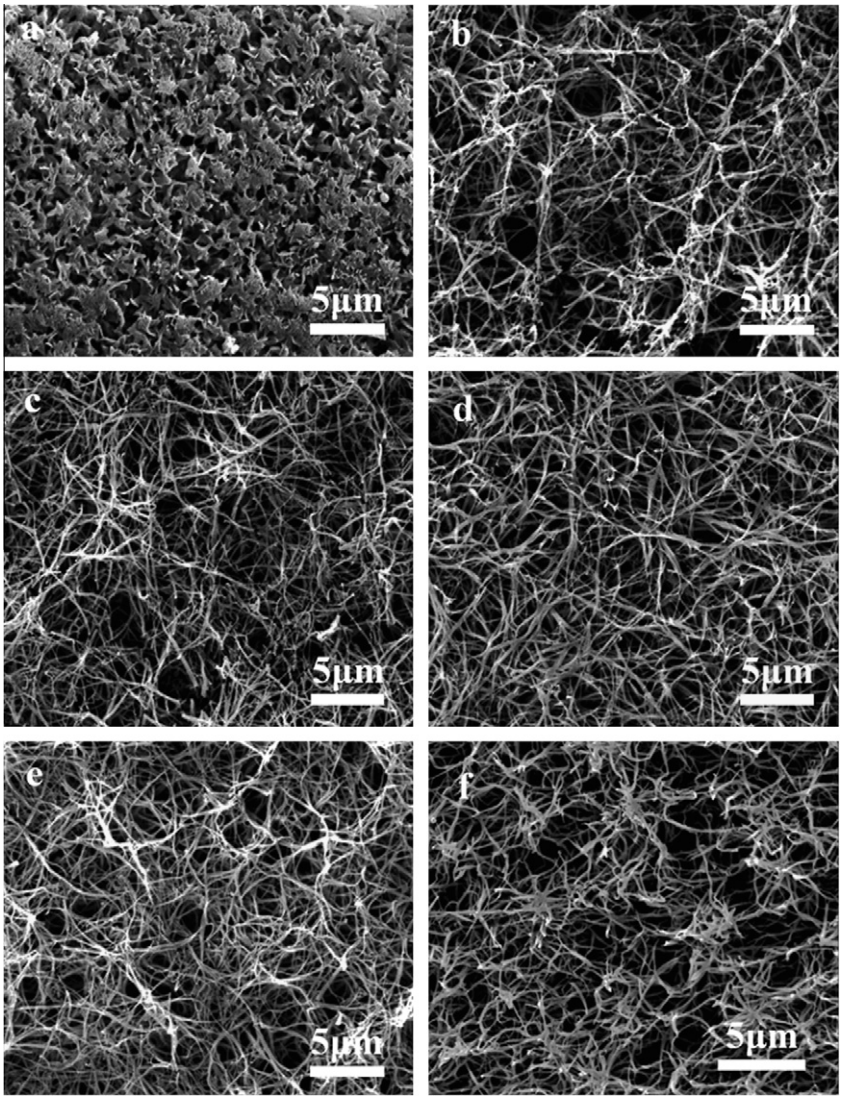

Fig. 1. SEM images of the various samples with different gelation time. (a) After quenching for 1 min, (b) 3 min, (c) 5 min, (d) 10 min, (e) 20 min and (f) 2 h.

3.2. WAXD patterns

The crystalline structure of PLLA with different quenching time was further investigated by WAXD analysis (Fig. 2). The degree of crystallinity was calculated as the percentage of the scattered intensity of the crystalline phase over the scattered intensity of the crystalline and amorphous phase [39]. An increase in the degree of crystallinity of PLLA with quenching time can be noted (Table 1). This crystallization process would result in more chain entanglement and decrease chain mobility. For comparison, all the diffraction patterns were normalized using the strongest (110)/(200) reflection intensity. Based on the two strongest reflections from (110)/(200) and (203), the crystalline phases were characterized as the α-form ($2\theta = 16.8°$ and 19.1°) at 1 min and the α′-form ($2\theta = 16.4°$ and 18.9°) at 10 min and thereafter [26–31], respectively. With the increase of the gelation time during 2 h, the two strongest reflections shift remarkably toward the lower 2θ side and then stabilized. The samples being quenched for 3 min and 5 min could be the mixture of α- and α′-phase. As reported previously, two relatively weak peaks at $2\theta = 14.9°$ and 22.4° for (010) and (211) reflections are the characteristic diffraction of the α-phase, whereas a quite small peak at $2\theta = 24.6°$ for (206) reflection is observed only in the α′-phase [26–31].

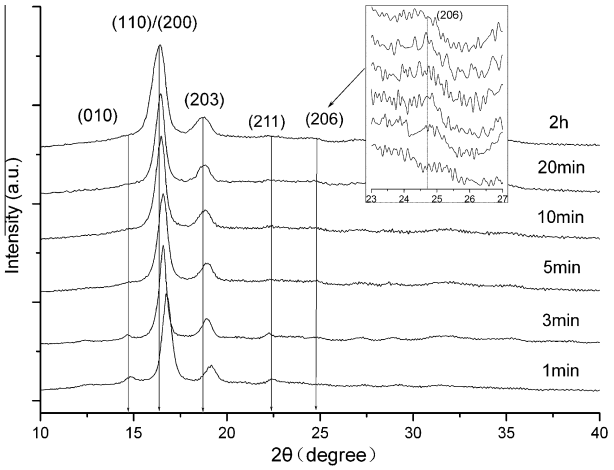

Fig. 2. WAXD patterns of the samples after 1 min, 3 min, 5 min, 10 min, 20 min and 2 h gelation.

The calculation of lattice spacings (d) of the (110)/(200) and (203) diffractions further confirmed the variation of phase structure of PLLA with different gelation time. The values of $d_{110/200}$

Table 1
The crystallinity, lattice spacing and contact angle of the samples with different gelation time.

Gelation time	WAXD			Contact angle (°)	DSC	
	χ_c (%)	$d_{110/200}$ (Å)	d_{203} (Å)		ΔH_m (J/g)	χ_c (%)
1 min	28.4 ± 6.0	5.283	4.627	91.9	24.8 ± 4.8	18.4 ± 3.6
3 min	32.7 ± 4.1	5.341	4.687	109.8	41.9 ± 0.6	31.1 ± 0.3
5 min	38.8 ± 1.5	5.342	4.692	115.7	47.1 ± 0.1	34.8 ± 0.1
10 min	40.8 ± 0.4	5.375	4.707	117.1	50.6 ± 3.9	37.3 ± 2.9
20 min	42.8 ± 1.2	5.388	4.712	128.9	53.3 ± 4.4	39.5 ± 3.3
2 h	53.1 ± 5.4	5.395	4.717	132.9	69.3 ± 6.4	51.4 ± 4.8

and d_{203} increase gradually with the gelation time (Table 1). The different gelation times determined the different temperatures under which the nucleation of PLLA crystals occurred from the amorphous gel. After quenching for 1 min, the temperature of the solution dropped to about 15 °C, and the temperature further decreased to about 0 °C after 2.5 min. The results suggested that α-form crystal is nucleated preferentially at higher temperature, while α′-form prevailed at lower temperatures. It has been reported that the α′-form is a limited disorder α-form with slightly different chain conformation and chain packing mode [29,30]. The WAXD results were consistent with the morphological observation. The morphological study of PLLA crystals from melt preparation also showed the lamellar morphology on a micrometer scale for the α-form crystal and fibrillar crystallites for the α′-form crystal [29–31,38].

3.3. DSC Analysis

Differential scanning calorimetry (DSC) measurements (Fig. 3) were carried out in the temperature range from room temperature to 200 °C at a heating rate of 10 °C/min under nitrogen gas flow. The degree of crystallinity was calculated as $\chi_c = \Delta H_m/\Delta H_m^0$, where ΔH_m was the measured enthalpy of melting and ΔH_m^0 was the enthalpy of melting of 100% crystalline polymer. For PLLA, $\Delta H_m^0 = 135\,J/g$ [40,41]. The calculated degree of crystallinity were comparable to the results of WAXD and showed a similar increasing trend with the increasing of the gelation time (Table 1).

3.4. ATR-FTIR spectrroscopy

ATR-FTIR was used for the further characterization of PLLA gelation and crystallization due to its distinct IR absorption patterns of amorphous and crystalline components in characteristic bands [31,42–44]. Fig. 4a shows IR spectra in the 1850–800 cm^{-1} region of various PLLA samples with different gelation time and the inset graph is the enlarged spectral region of 980–840 cm^{-1}. Two small bands at 921 cm^{-1} and 955 cm^{-1} which ascribed to a 10_3 helix sensitive crystallization band and an amorphous band, respectively [20,31,44], can be clearly observed in all spectra. The presence of β-crystal can be ruled out by the absence of the characteristic band at 908 cm^{-1} in all spectra [31]. Fig. 4b shows the overlapped spectra which were normalized according to the peak at 1454 cm^{-1} (see below for a detailed discussion).

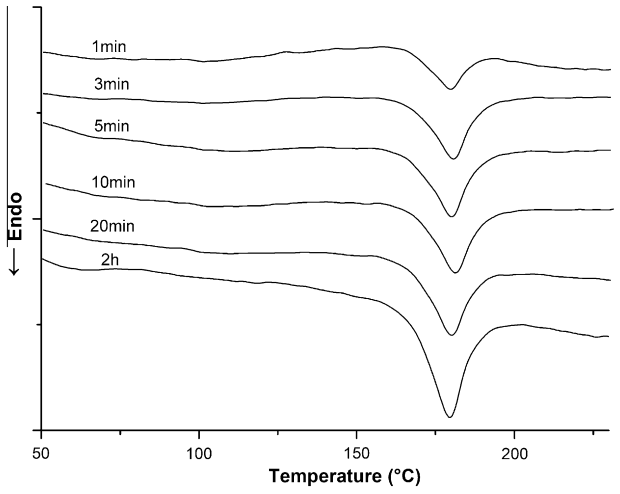

Fig. 3. DSC curves of the samples after 1 min, 3 min, 5 min, 10 min, 20 min and 2 h gelation.

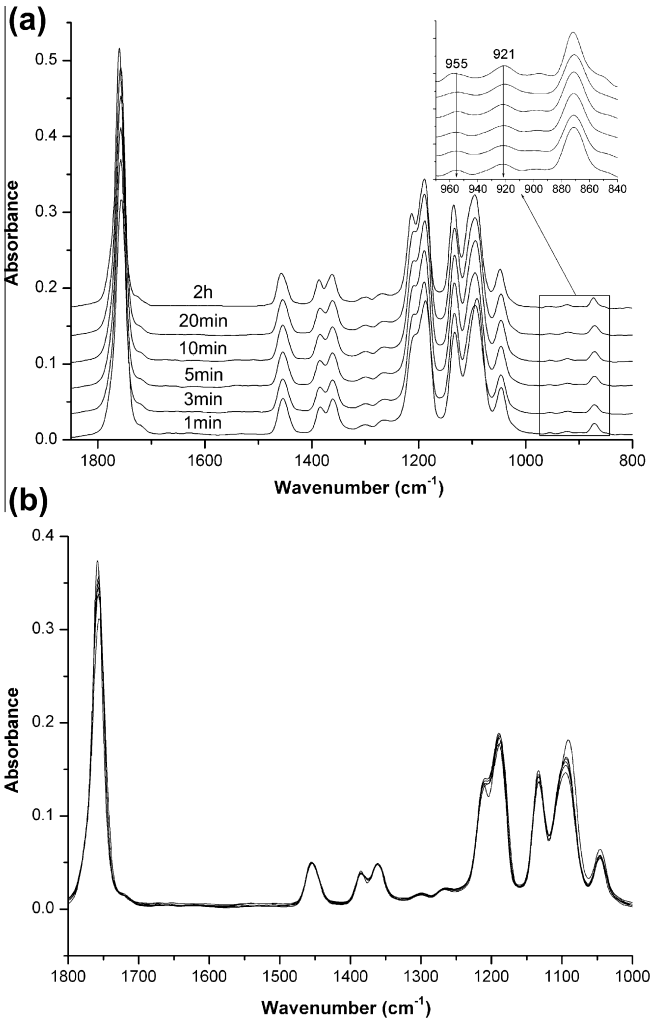

Fig. 4. (a) ATR-FTIR spectra in the range 1850–800 cm^{-1} of various PLLA samples with different gelation time. The inset graph is the enlarged spectral region of 980–840 cm^{-1}. (b) The overlapped spectra which were normalized according to the peak at 1454 cm^{-1}.

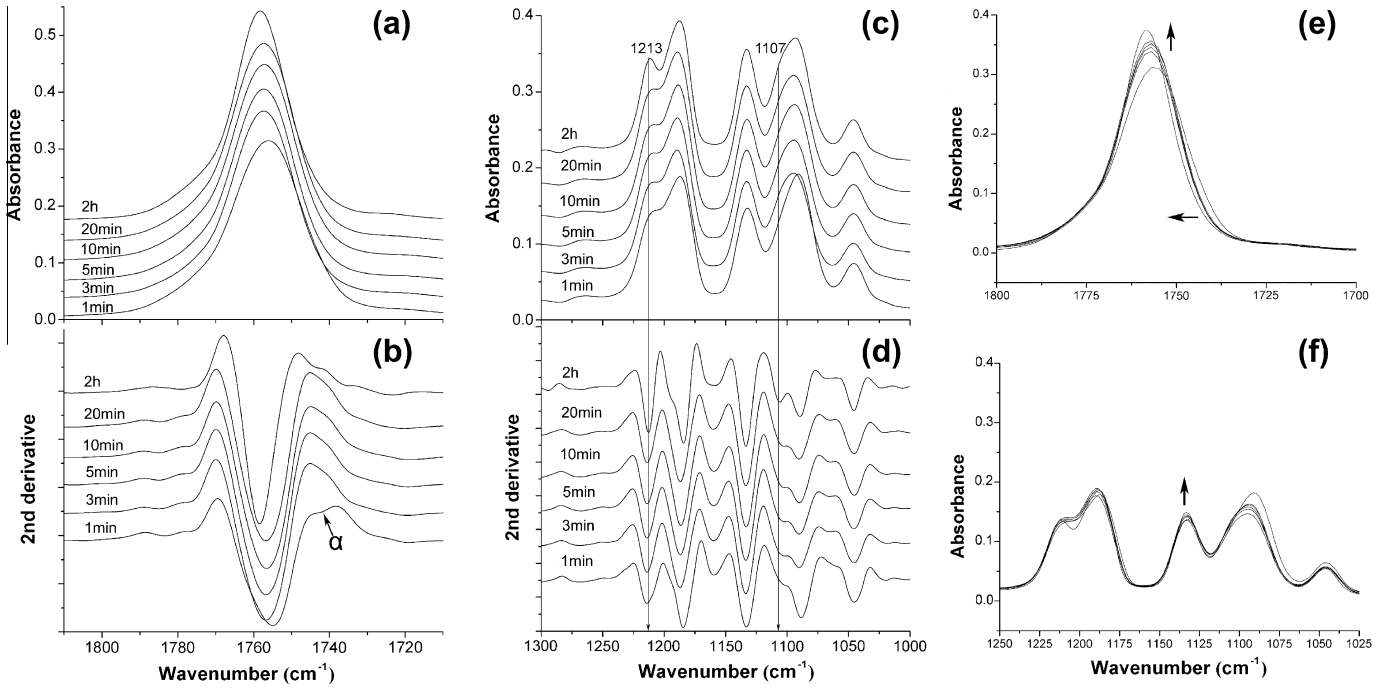

Fig. 5. ATR-FTIR spectra and corresponding second derivative spectra in the ranges of (a and b) 1810–1710 cm^{-1} and (c and d) 1300–1000 cm^{-1} for the PLLA samples with different gelation time. The enlarged spectra in the ranges of (e) 1800–1700 cm^{-1} and (f) 1250–1025 cm^{-1} which were normalized according to the peak at 1454 cm^{-1}.

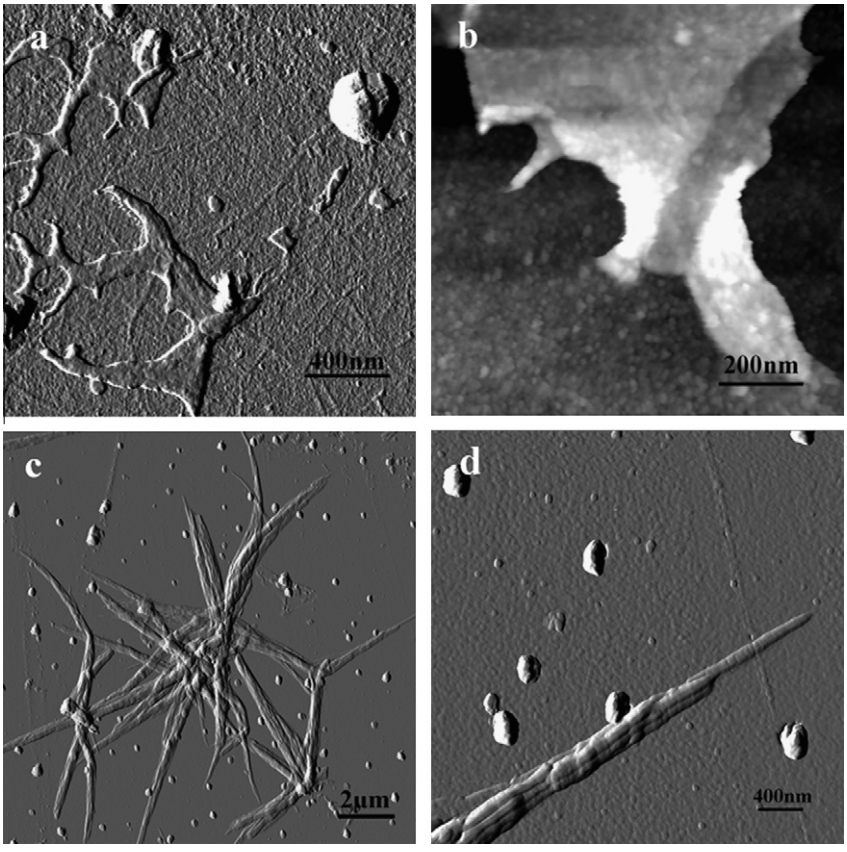

Fig. 6. Typical AFM images of PLLA precipitates after 2 min (a and b) and 10 min (c and d) gelation. Patches of amorphous precipitates from the condensation of nanoparticles were prevailed in the early stage of phase separation process. The nanofibers appeared to have a central nuclei and grew radially outward. The lateral assembly of thinner nanofibers into larger ones was evident.

Fig. 5a–d shows the spectra and the corresponding second derivative spectra in 1810–1710 cm^{-1} and 1300–1000 cm^{-1} ranges respectively. The splitting band characteristic for α-crystal around 1745 cm^{-1}, attribute to the carbonyl stretching vibration [ν(C=O)],

was evident in the spectra of the sample of 1 min quenching. All the other spectra display a crystalline band located at about 1755 cm^{-1}, attributed to the C=O stretching mode for α′-form [43–45]. The stretching vibration of C—O—C bond and rocking vibration of CH_3 bonds are presented in 1300–1000 cm^{-1} range [26]. It is clear that two bands at about 1213 cm^{-1} and 1187 cm^{-1} related to the $\nu_{as}(C—O—C) + r_{as}(CH_3)$ and $\nu_{as}(C—O—C)$ respectively have become sharper and more distinctly with increasing gelation time. The sharpening of these peaks could be due to the increasing of the crystallinity degree, which is consistent with the WAXD data. The peak at about 1454 cm^{-1} is assigned to the stretching asymmetric vibrations mode of C—H in methyl groups and can be used as an internal standard to normalize all the spectra [46]. As shown by the overlapped spectra in Fig. 5e, the intensity of the C=O stretching band at about 1755 cm^{-1} increased with the gelation time. A shift toward higher wavenumber for this band can also be observed. The high-frequency shift of this specific vibration suggested a stiffer segmental motions and stronger interactions between the related segments. Since the bands at 1755 cm^{-1} represent the crystalline components of PLLA [42], the results can therefore be attributed to the increase of crystallinity. Moreover, the high-frequency shift of the C=O stretching band is likely due to the interchain dipole coupling of the C=O bonds in the crystalline state [44]. As reported that the C=O stretching band for α′-phase located at higher wavenumber than it for α-phase. The phenomena is consistent with the result of WAXD that the α′-phase crystal prevailed with the increasing gelation time. As shown in Fig. 5f, the intensity of the C—O—C symmetric stretching mode at about 1090 cm^{-1} exhibited a decreasing trend suggesting a more closely packed polymer segments that restricted the backbone vibration. The intensity change of these peaks confirmed the change in the chain conformation of the samples from different gelation time. Furthermore, a slight increase in the intensity of the band at 1132 cm^{-1} was observed. This band was assigned to CH_3 rocking vibrations. In a study of the solution cast PLLA films by using ATR-FTIR and the transmission FTIR, Thanki et al. considered the intensity increase of this band in ATR-FTIR spectra as an indication for the surface segregation of the methyl groups in the films [46]. In the current study, the possible surface segregation of the methyl groups was confirmed by X-ray photoelectron spectroscopy (XPS) analysis which allows the determination of the chemical composition of the sample surface of about 10 nm depth. The relative composition of the C1s of aliphatic carbon bonds or carbon-hydrogen bonds increased with the increasing gelation time (data not shown).

3.5. Contact angle measurement

Contact angle of water droplet was measured by sessile drop method and the value was reported in Table 1. All the samples were pressed into films with similar roughness (less than 1 μm). The water contact angle of the samples increased along with the

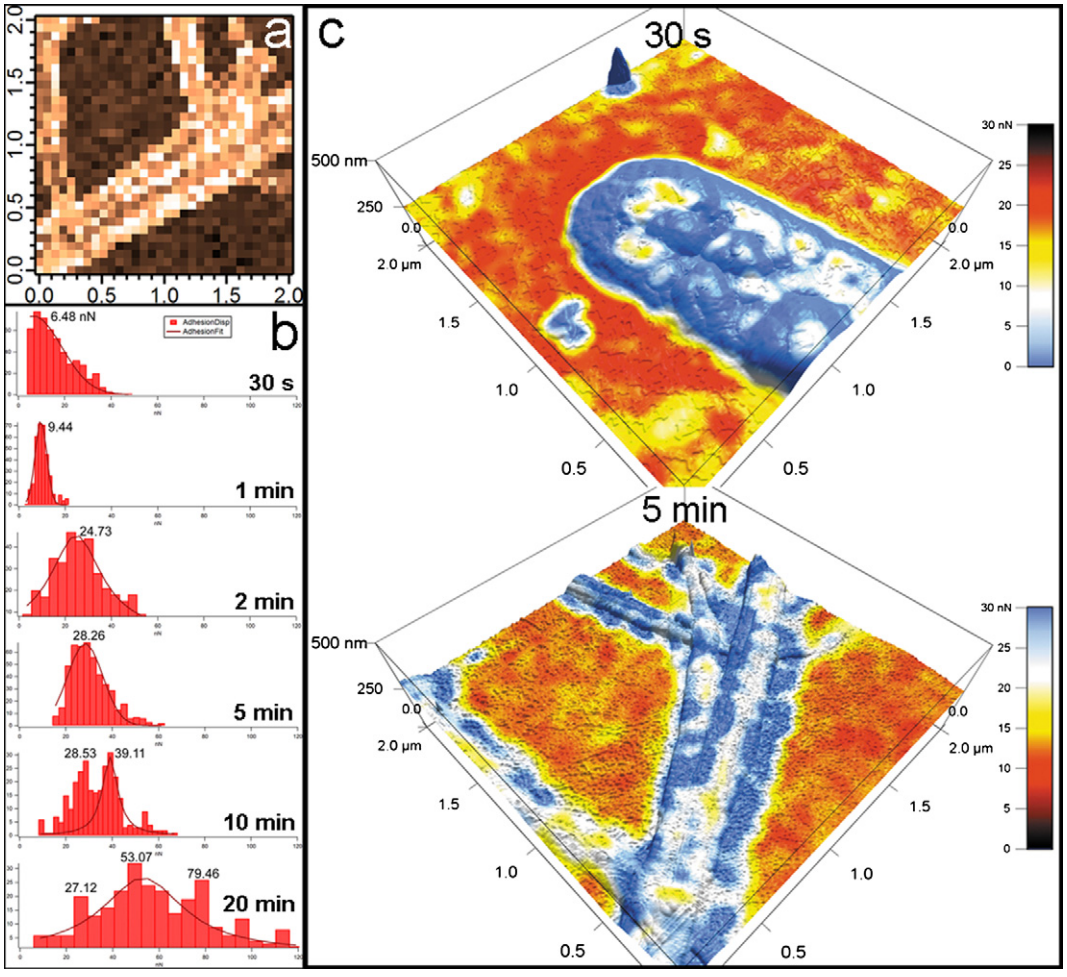

Fig. 7. (a) A representative 2 × 2 μm^2 force-map (32 points over 32 lines) of the sample after 5 min gelation. The brighter region shows the position of nanofibers. (b) The frequency histograms of adhesion forces with the Gaussian fitting curves of the samples. (c) Typical 3D overlayed images of adding a force map image (color) onto the topography image corresponding to samples of 30 s and 5 min respectively. (For interpretation of the references to colour in this figure legend, the reader is referred to the web version of this article.)

Table 2
The most probable adhesion forces and other peak values of high probability of the samples with different gelation time.

Gelation time	30 s	1 min	2 min	5 min	10 min		20 min		
Mean (nN)	6.48	9.44	24.73	28.26	28.53	39.11	27.12	53.07	79.46
Width (nN)	10.78	2.56	9.27	8.43	5.36	6.11	6.89	18.63	6.29

gelation process. The porous surface morphology and the surface chemistry of the possible segregation of the hydrophobic methyl groups during the gelation process played important roles in the increase of the hydrophobicity.

3.6. AFM

We further investigated the evolution of nanofibrous texture during the early stages of TIPS process by atomic force microscopy (AFM) and force spectroscopy measurements (MFP-3D AFM, Asylum Research, Santa Barbara, CA). A diluted 0.5% (w/v) PLLA/THF solution was prepared to cast 2-D samples on the glass slide for the study. A series of samples with different quenching time (30 s, 1 min, 2 min, 5 min, 10 min and 20 min) at −24 °C were obtained following the same procedures. Comparing to the 3-D samples, these samples had a higher quenching rate and thus represent the lower temperature behavior of PLLA gelation. In general, patches of amorphous precipitates prevailed within 2 min quenching and thereafter nanofibrous structure were abundant. Fig. 6 shows the typical images of 2 min (Fig. 6a and b) and 10 min (Fig. 6c and d) samples, respectively. The condensation of amorphous nanoparticles of about 20 nm in diameter was evident in the early stage of phase separation process (Fig. 6b). The nanofiber formation seemed to initiate from a central nuclei and grew radially outward (Fig. 6c). It is clear that a bunch of thinner nanofibers of about 100 nm in diameter assembled laterally into larger nanofibers (Fig. 6d).

3.7. Force spectroscopy measurement

Force spectroscopy measurements were performed under contact mode using silicon nitride probes. The cantilever spring constants were determined to be 1.39 nN/nm with the thermal noise method. A force-map (32 points over 32 lines) was recorded over a $2 \times 2\ \mu m^2$ area of interest (Fig. 7a). The probe position was raster scanned over the sample surface after each force plot. Force-distance curves collected at each probe position were digitally stored for subsequent analysis and the value of adhesion force can be determined using MFP-3D software. From a force map, about 300 individual force spectra within the area of the amorphous precipitates (the 30 s, 1 min and 2 min samples) or nanofibers (the 5 min, 10 min and 20 min samples) can be extracted to produce a probability histogram of adhesion force as shown in Fig. 7b. The histogram was fitted by the Gaussian curve and the position of the maximum of the Gaussian component was taken as the most probable force [47]. Table 2 shows the most probable adhesion forces and other peak forces of high probability on the different samples as well as the width of variation.

Basically, the adhesion force between the AFM probe and sample surfaces obtained in atmospheric air is the superposition of van der Waals, electrostatic, and capillary and interfacial tension forces. The capillary and interfacial tension forces were due to the formation of the capillary water bridge and strongly dependent on the surface hydrophilicity. Under the conditions of a good hydrophobicity with the contact angle greater than 100° and an air humidity less than 50%, the contributions of capillary and superficial tension forces were minimized and the van der Waals and solid–solid interfacial forces can be regarded as major contributors to the adhesion force [37]. It is apparent that the most probable adhesion force between the AFM probes and the polymer precipitates increased with the gelation time. This is a clear demonstration that the structural evolution of PLLA chains conformation and chain packing mode has a direct functional consequence in the nanoscale mechnical property. Moreover, multipeaks of high probability adhesion force besides the most probable one can be noted from the nanofiber samples of 10 min and 20 min. This increased heterogeneity in the adhesion forces can be attributed to the structural adjustment of the nanofibers during their assembling process.

Fig. 7c shows two typical 3D overlayed images of adding a force map image (color)[1] on to the topography image corresponding to samples of 30 s and 5 min respectively. Topography images were obtained from the height channel of AC mode (tapping mode) images right before the force spectroscopy measurement. A heterogeneity of the adhesion forces within both amorphous precipitate (30 s) and nanofibers (5 min) were apparent.

4. Conclusions

In summary, the early stage of PLLA nanofibers formation via thermally induced phase separation process involved the condensation of amorphous nanoparticles and a gradual crystallization from the gel. With extending the gel process, a microporous structure can be formed. A temperature dependent phase behavior during the early quenching period has been observed. The α-form crystal appeared after quenching for 1 min, corresponding to a gel temperature around 15 °C. After quenching for sufficient time to decrease the gel temperature below 0 °C, a limited disorder α′-form crystal prevailed and the content of α′-phase in the mixture was increasing gradually with the gelation time. Along with the increase in the degree of crystallinity, structural transformation of the polymer toward a more ordered and compact state proceeded with the extending of the gelation time. The surface morphology and conformational changes of the polymer chains had effect of increasing the hydrophobicity and nanoscale mechanical property. The adhesion force increased with the gelation time which suggested that the structural evolution of PLLA chains conformation and the chain packing has a direct functional consequence in the nanoscale mechanical property.

Acknowledgements

The work was financially supported by National Basic Research Program of China (2012CB619100), National Natural Science Foundation of China (51072056), Program for New Century Excellent Talents in University (NCET-08-0210), Program for Changjiang Scholars and Innovative Research Team in University (IRT 0919) and Guangdong Provincial Scientific Funds (2010B090400324).

References

[1] M.M. Stevens, J.H. George, Science 310 (2005) 1135–1138.
[2] K.M. Woo, J. Jun, V.J. Chen, J. Seo, J.H. Baek, H.M. Ryoo, G.S. Kim, M.J. Somerman, P.X. Ma, Biomaterials 28 (2007) 335–343.

[1] For interpretation of color in Fig. 7, the reader is referred to the web version of this article.

[3] J.W. Xie, X.R. Li, Y.N. Xia, Macromol. Rapid Commun. 29 (2008) 1775–1792.
[4] L.A. Smith, P.X. Ma, Collold. Surf. B:Biointerf. 39 (2004) 125–131.
[5] A. Nur-E-Kamal, I. Ahmed, J. Kamal, M. Sehindler, S. Meiners, Biochem. Biophys. Res. Commun. 331 (2005) 428–434.
[6] J.D. Hartgerink, E. Beniash, S.I. Stupp, Science 294 (2001) 1684–1688.
[7] J.S. Qian, M. Zhang, I. Manners, M.A. Winnik, Trends Biotechnol. 28 (2010) 84–92.
[8] T. Koga, T. Watanabe, N. Higashi, J. Nanosci. Nanotechnol. 9 (2009) 584–590.
[9] P.F. Duan, M.H. Liu, Langmuir 25 (2009) 8706–8713.
[10] H. Yoshimoto, Y.M. Shin, H. Terai, J.P. Vacanti, Biomaterials 24 (2003) 2077–2082.
[11] Z.M. Huang, Y.Z. Zhang, M. Kotaki, S. Ramakrishna, Compos. Sci. Technol. 63 (2003) 2223–2253.
[12] F. Yang, R. Murugan, S. Wang, S. Ramakrishna, Biomaterials 26 (2005) 2603–2610.
[13] L.A. Smith, X.H. Liu, P.X. Ma, Soft Matter 4 (2008) 2144–2149.
[14] L.M. He, Y.Q. Zhang, X. Zeng, Polymer 50 (2009) 4128–4138.
[15] P.X. Ma, R.J. Zhang, Biomed. Mater. Res. 46 (1999) 60–72.
[16] F. Yang, R. Murugan, S. Ramakrishna, X. Wang, Y.X. Ma, S. Wang, Biomaterials 25 (2004) 1891–1900.
[17] X.T. Li, Y. Zhang, G.Q. Chen, Biomaterials 29 (2008) 3720–3728.
[18] E.D. Hay, Cell Biology of Extracellular Matrix, second ed., Plenum Press, New York, 1991.
[19] S. Sasaki, T. Asakura, Macromolecules 36 (2003) 8385–8390.
[20] D. Sawai, K. Takahashi, A. Sasashige, T. Kanamoto, Macromolecules 36 (2003) 3601–3605.
[21] T. Miyata, T. Masuko, Polymer 38 (1997) 4003–4009.
[22] W. Hoogsteen, A.R. Postema, A.J. Pennings, G. Ten Brinke, Macromolecules 23 (1990) 634–642.
[23] L. Cartier, T. Okihara, Y. Ikada, H. Tsuji, J. Puiggali, B. Lotz, Polymer 41 (2000) 8909–8919.
[24] T. Kawai, N. Rahman, G. Matsuba, K. Nishida, T. Kanaya, M. Nakano, et al., Macromolecules 40 (2007) 9463–9469.
[25] Y. Hu, H. Sato, J. Zhang, I. Nada, Y. Ozaki, Polymer 49 (2008) 4204–4210.
[26] P. Pan, B. Zhu, W. Kai, T. Dong, Y. Inoue, Macromolecules 41 (2008) 4296–4304.
[27] P. Pan, Z. Liang, B. Zhu, T. Dong, Y. Inoue, Macromolecules 42 (2009) 3374–3380.
[28] P. Pan, W. Kai, B. Zhu, T. Dong, Y. Inoue, Macromolecules 40 (2007) 6898–6905.
[29] H. Marubayashi, S. Akaishi, S. Akasaka, Macromolecules 41 (2008) 9192–9203.
[30] J. Zhang, K. Tashiro, H. Tsuji, A.J. Domb, Macromolecules 41 (2008) 1352–1357.
[31] J. Zhang, Y. Duan, H. Sato, H. Tsuji, I. Noda, S. Yan, Y. Ozaki, Macromolecules 38 (2005) 8012–8021.
[32] S.H. Kim, Y.S. Nam, T.S. Lee, W.H. Park, Polym. J. 35 (2003) 185–190.
[33] E.P.S. Tan, C.T. Lim, Appl. Phys. Lett. 84 (2004) 1603–1605.
[34] E.P.S. Tan, C.T. Lim, Appl. Phys. Lett. 87 (2005) 123106.
[35] C.A. Grant, D.J. Brockwell, S.E. Radford, N.H. Thomson, Appl. Phys. Lett. 92 (2008) 233902.
[36] K. Sugisaki, K. Nakano, H. Sugimura, N. Kandaka, N. Nakagiri, Jpn. J. Appl. Phys. 37 (1998) 3820–3823.
[37] L. Sirghi, M. Nakamura, Y. Hatanaka, O. Takai, Langmuir 17 (2001) 8199–8203.
[38] C. Alemán, B. Lotz, J. Puiggali, Macromolecules 34 (2001) 4795–4801.
[39] J.S.C. Loo, C.P. Ooi, F.Y.C. Boey, Biomaterials 26 (2005) 1359–1367.
[40] T. Miyata, T. Masuko, Polymer 39 (1998) 5515–5521.
[41] S. Sosnowski, Polymer 42 (2001) 637–643.
[42] T. Furukawa, H. Sato, R. Murakami, J. Zhang, I. Noda, Polymer 48 (2007) 1749–1755.
[43] J. Zhang, Y. Duan, A.J. Domb, Y. Ozaki, Macromolecules 43 (2010) 4240–4246.
[44] J. Zhang, H. Tsuji, I. Noda, Y. Ozaki, Macromolecules 37 (2004) 6433–6439.
[45] E. Meaurio, I. Martinez de Arenaza, E. Lizundia, J.R. Sarasua, Macromolecules 42 (2009) 5717–5727.
[46] P.N. Thanki, E. Dellacherie, J.-L. Six, Appl. Surf. Sci. 253 (2006) 2758–2764.
[47] C. Ray, J.R. Brown, B.B. Akhremitchev, Langmuir 23 (2007) 6076–6083.